Journal of Undergraduate Chemistry Research, **2026**, 25 (1), 7

Δ-TOF MASS SPECTROMETRY – TOPOGRAPHIC SURFACE IMAGING BY MATRIX-ASSISTED LASER DESORPTION/IONIZATION TIME-OF-FLIGHT

Varun Kadiyala* and Andreas H. Franz†

Department of Chemistry, University of the Pacific, Stockton, CA 95211

Abstract

Mass spectrometry produces structural information from minute amounts of material and requires mass accuracy achieved by calibrating the instrument. Here, a method is presented that only relies on precision but not accuracy. The method, which we call MALDI-Δ-TOF mass spectrometry, acquires mass spectral data in a Time-Of-Flight (TOF) detector, which provides surface images including topographic information (elevations and depressions). The method exploits minute differences in flight time of ions that are generated under identical instrumental conditions from elevated or depressed areas of the surface. The surface topography is reconstructed from extracted image slices in the *m/z*-dimension in 0.1-unit increments.

†Corresponding author: afranz@pacific.edu *Undergraduate researcher and co-author

Keywords: Matrix-Assisted Laser Desorption/Ionization (MALDI), time-of-flight mass spectrometry, Δ-TOF imaging, matrix sublimation

Received: January 4, 2026 Accepted: January 10, 2026 Revision received: January 11, 2026 Published: January 15, 2026

Introduction

After its introduction by Karas *et al.* 40 years ago [1] and its combination with Time-Of-Flight (TOF) mass analyzers from the late 1940s,[2-3] Matrix-Assisted Laser Desorption/Ionization (MALDI) TOF mass spectrometry (MS)[4] has become an invaluable analytical technique in clinical research and was included in the 2002 chemistry Nobel Prize for structural analysis of biological macromolecules.[5] Its value has been demonstrated in pathogen detection,[6-7] in clinical diagnostics,[8-11] in nucleic acid analysis,[12-13] and in small molecule detection.[14] The analyte of interest is co-crystallized with a "matrix", which is typically a UV-active small molecule substance, which absorbs the laser light to assist in thermal/photo ionization and desorption of the analyte molecule from the surface of the target plate.

MALDI-TOF MS and the related technique MALDI Secondary Ion Mass Spectrometry (SIMS)[15-16] TOF MS have been used to characterize spatial composition of surfaces, including surface topography, [17-18] with the help of small molecules and biomolecules (MALDI-imaging).[19-20] While MALDI-TOF MS has the advantage of ionizing larger molecules, MALDI-SIMS on the other hand provides superior resolution.[21] Surface images are generated from thousands of MS-spectra collected row-by-row after deposition of matrix onto the surface via spraying or sublimation. The former is simpler to carry out; the latter is superior in microscopic crystal size and sensitivity. Very recently, research has shown that different compound classes ionize from samples prepared by either one of the two techniques.[22] The focus of imaging experiments is to detect the distribution of specific compounds with high mass accuracy for unambiguous compound identification. Proper calibration of the *m/z*-axis is essential for mass accuracy and is "*non plus ultra*" for unambiguous compound identification. However, we will argue that a quantity of *difference* between two not necessarily accurate measurements can also be valuable, provided the measurements were precise. Differences in time-of-flight have the potential to reveal the topography of a surface as elevations (shorter flight time to the detector) versus depressions (longer flight time to the detector). While surface profiles can be revealed with near unparalleled precision by advanced microscopic techniques such as confocal laser scanning microscopy (CLSM), mass spectrometry has the power of identifying many individual ionized compounds from one sample. If differences in flight time of those ions can be used to describe the surface location from where the ions originated, advanced description of the topography *and* chemical composition of surfaces of biological objects may be possible.

Here, we describe how MALDI-TOF MS can be used to extract surface topography information in time-dispersion. We call it MALDI-Δ-TOF MS. We also describe an inexpensive sublimation apparatus for matrix deposition onto heat-resistant surfaces. Data quality and limitations of the technique will be discussed.

Experimental

MALDI matrices were purchased from SIGMA-ALDRICH and were used for sublimation without further purification (α-cyano-4-hydroxycinnamic acid [CHCA, 97%], 2,5-dihydroxybenzoic acid [DHB, 97%)], and 3-picolinic acid [3-PA, 97%]). All MALDI experiments were carried out on a Shimadzu AXIMA Performance instrument (spectral processing: Launchpad 2.9.3) The instrument was operated at room temperature with an N_2-laser (λ = 337 nm, 120 μJ/pulse) at ~8 * 10^{-7} torr. Unless stated otherwise, samples were applied to a stainless-steel MALDI plate in 96-well format or 384-well format. The standard "dried droplet" method was used for sample preparation. Droplets were allowed to evaporate slowly at room temperature in non-turbulent air. Samples were also prepared by matrix deposition by re-sublimation.

MALDI-TOF acquisition

Standard spectra were acquired by collecting 200 profiles with 10 laser pulses/profile. During acquisition, the laser position was manually adjusted to collect data from locations with adequate ion production. The laser attenuator was set to just above the threshold of ion formation. Ions were extracted with 20.0 kV acceleration potential after a 115.0 ns delay for collisional cooling and einzel lens focusing with 6.5 kV. The deflector voltages for the ion beam in X- and Y-direction were -31.0 V and +65.0 V in linear mode, respectively. When operating the reflectron at 24.4 kV, the additional deflector voltages for the ion beam in X- and Y-direction

were -90.0 V and 0.0 V, respectively. The detector voltages were 2.38 kV in linear mode and 2.20 kV in reflectron mode.

Matrix sublimation

The matrix (~100 mg) was placed into a tea candlelight aluminum cup covered with aluminum foil (dull side facing the matrix), which was held in place by a metal weight (Fig. S5). A box cutter blade with defined pattern (stencil) was overlayed onto the aluminum foil and the matrix. The assembly was placed into a stainless-steel vessel that was subsequently evacuated by an oil pump. After 5-10 minutes of evacuation, with the pump running, the vacuum vessel was placed carefully on a standard laboratory heat plate that was pre-heated to 180-200 °C. The apparatus was heated for 3-5 minutes, depending on desired matrix layer thickness, and was then removed from the heat plate. The vessel was vented slowly, and the weight and the aluminum foil were removed carefully with forceps. The aluminum foil was then attached to a standard MALDI sample plate with small pieces of tape. Coins for imaging were thoroughly cleaned prior to matrix sublimation. Briefly, the coins were placed in a beaker with methanol. The coins were sonicated for 15 minutes. The procedure was repeated twice, and the coins were dried on paper towel.

MALDI-imaging

The dimensions of the area to be imaged were defined by X-/Y-coordinates, and the number of image pixels (laser shot locations, $z = f_{(x,y)}$) was calculated based on a spacing of 80 μm between columns and rows of the TV-raster. An area of 5 x 5 mm required approximately 4,000 profiles and was analyzed with 2 laser shots per profile. The ink stick figures were analyzed with 10 laser shots per spot. All spectra were saved and used for image generation. Ion images were displayed in Total Ion Current (TIC) mode or in Sum Masses mode. Within one *m/z*-unit window, ten *m/z*-specific TIC images were extracted with ± 0.1 Da tolerance and exported as ASCII text files. Each intensity column (z) was filtered for values above a set threshold. Values that met the threshold limit were replaced with the *m/z*-value for which the image was extracted. The other values were set to a value 0.1 *m/z*-units below the threshold. The resulting data block consisting of x-column, y-column, and ten filtered z-columns was displayed as topographic XYZ-surface in irregular form with 300 grid data points in each x- and y-dimension with an *m/z*-dependent color gradient (PSI-Plot, Ver. 8.02, Poly Software International, Inc).

Results and Discussion

General MALDI-TOF Imaging Experiments

The simplest successful imaging results were obtained by using substances that ionize easily by themselves without the help of matrix. The ink used in everyday ball point pens ionized efficiently off the MALDI plate, and a total of 11,667 spectra were recorded. Whereas blue and black ink gave very strong ion response, the red ink was much less sensitive even though the figures were drawn with similar amounts of ink (Fig. S1). The absolute ion count was substance-dependent, which made direct quantification impossible without an ion-intensity calibration curve. The non-uniform ink distribution caused obvious differences in the ion intensity map. Line features that were spaced apart approximately 80 μm or more were successfully resolved (Fig. S2). This finding was consistent with a laser beam diameter of approximately 50 μm as specified by the manufacturer. Extracted ion images for specific *m/z*-values (Fig. S3) allowed identification of which figure was drawn with which color (Fig. S4).

Matrix sublimation and evaluation of sample quality

The in-house sublimation apparatus (Fig. S5) produced matrix deposits with excellent microscopic crystal size (Fig. S6). The matrix layer was thin enough to be depleted by repeated laser shots (Fig. S7), and ionization efficiency (Total Ion Current, TIC) was near uniform across areas defined by the box cutter stencil (Fig. S8). We found that 3-4 minutes of sublimation gave the best results. Shorter times gave irregular TIC response and was not useful for imaging. One disadvantage of the sublimation apparatus was the lack of sample cooling during resublimation. In the vacuum chamber all thermal energy from resublimation was transferred to the object's surface. At temperatures of 180-200 °C, the method was only applicable to heat-resistant materials. It was incompatible with biological samples.

Principle of MALDI-Δ-TOF Experiments

We explored how to display the intensity-dependent mass spectral images (detector ion count), in an *m/z*-dependent format. MALDI-TOF images were extracted for specific *m/z*-values in increments of 0.1 ± 0.05 *m/z*-unit tolerance. For the stick figure in blue ink, we chose the *m/z* range of 361.0-361.9 to avoid sampling the subsequent isotope peak around *m/z* 362 (Fig. 1). For each of the 11,667 spots in the image, we translated the intensity image into a surface profile based on flight time differences, and we will refer to it as Δ-TOF.

The inverse relationship between surface elevation and ion flight time resulted in higher *m/z*-values for longer flight times, that is for ions that originated from surface *depressions*, whereas the opposite was true for ions originating from surface elevations. In order to represent elevations and depressions correctly in the ion image, the x,y-plane of the plot had to be flipped 180 °. Consequentially, the image became a mirror image (Fig. 1).

To test whether these flight-time differences could be useful in topographic mapping of uneven surfaces in general, we started with dried droplets that were applied to a simple staircase of two thin metal plates laid on top of each other (Fig. S9). Both dried droplets were imaged by a standard TV-raster (100 μm spacing, 3040 points). The ionization efficiency was found to be excellent and near uniform across both spots resulting in well-defined spatial outline of the spots (Fig. S10). Extraction of ion images for specific *m/z*-value gave layers that showed how the ions were distributed between the two spots (Fig. 2).

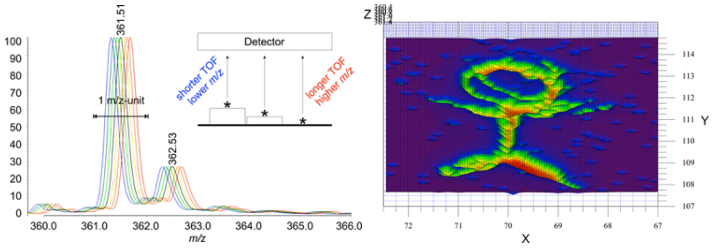

Figure 1. Δ-TOF image showing the depletion of ink where 10 laser shots hit (Z-axis: *m/z*). Note that the image (Fig. 1S) is mirrored because profile data show longer flight time as depression.

All spots of the raster were irradiated with 10 laser pulses each, which burned holes into the surface and caused a distribution of flight times progressively longer as the holes grew deeper (Fig. 2 and Fig. S11). This was identical for all locations probed by the laser during rastering. Integration of all *m/z*-layers allowed reconstruction of the isotope pattern of the protonated CHCA molecule. There was a distinct spatial *vertical* difference between ion populations from the lower level (longer flight time, higher *m/z*-value) and ions from the higher level (shorter flight time, lower *m/z*-value) of Δ *m/z* ~0.5. If the flight time difference in Δ *m/z* was less than ±0.5, so that oversampling of adjacent isotope peaks at ±1 Da was avoided, then general surface features were detected. Interestingly, when we plotted the Δ-TOF images along the *m/z*-axis, we saw that the periphery of the spot was characterized by shorter flight times whereas part of the center of the spot showed longer flight times (Fig. 3). This implied that the center of the spot had less matrix crystals (depression) whereas the periphery was elevated because of a thicker crystal deposit, which was a direct consequence of how crystallization progressed during droplet evaporation.

The droplet shape and the physical process of droplet evaporation is complex and depends on the hydrophobicity of the surface from which the droplet evaporates. Mathematical models have been described that postulate higher rate of evaporation at the periphery of a droplet if the drop's contact angle with the surface is small ($0^o < \theta < 90^o$) and the droplet has parabola shape [23]. The underlying assumption is that the droplet evaporates in a quiet atmosphere (non-turbulent air) and that the process of evaporation is quasi-steady. In such a scenario a radial centrosymmetric concentration gradient of matrix should develop, and more material will crystallize at the periphery as was observed in our case.

We then turned our attention to the analysis of CHCA that had been resublimed onto aluminum foil. We observed slight differences in layer thickness, which were found consistent with visible features in the microscopic picture of the matrix deposit (Fig. 4, top).

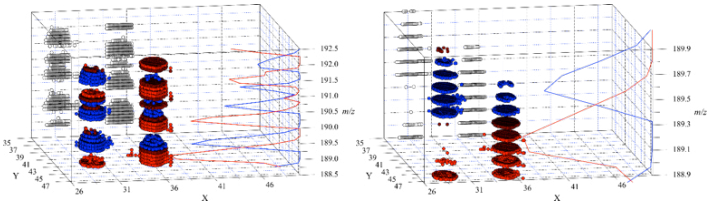

Figure 2. Layers of extracted ion images (*m/z* 188.9 – 192.0 in increments of 0.1) showing the two distinct locations of the matrix spots in the X-Y-plane of the target plate. Integration of all *m/z*-layers allowed reconstruction of the matrix ion isotope pattern and showed the spatial *vertical* difference of the spot on the lower level (longer flight time, higher *m/z*-value) and the spot on the higher level (shorter flight time, lower *m/z*-value) of Δ *m/z* ~0.5.

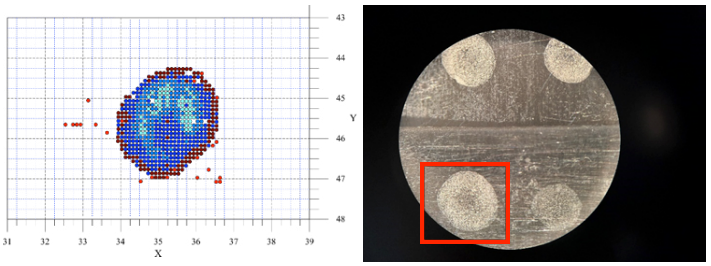

Figure 3. Left: Vertical plot along the *m/z*-axis showing the spatial distribution of ions with specific *m/z*-value (purple: *m/z* 189.3, blue: *m/z* 189.4, cyan: *m/z* 189.5, teal: *m/z* 189.6). The Δ-TOF surface topography suggested that the droplet had a concave surface towards the droplet's center consistent with the light microscopic picture of the spot (right).

Therefore, a topographic profile of the imaged object was generated based on differences in flight time of simple matrix reporter ions. Likewise, we generated a Δ-TOF image of a fingerprint on aluminum foil with the help of DHB matrix sublimation (Fig. 4, bottom). In areas with less matrix deposition the DHB ion flight times were longer as opposed to parts with thicker matrix layer.

Topographic MALDI-Δ-TOF Imaging Experiments

To verify that the principle of Δ-TOF can be applied to more complicated surfaces, we sublimed CHCA matrix onto the surface of metal coins (Fig. 5A). We found it advantageous to image with only 2 laser pulses per profile as opposed to 10 pulses. Fewer laser

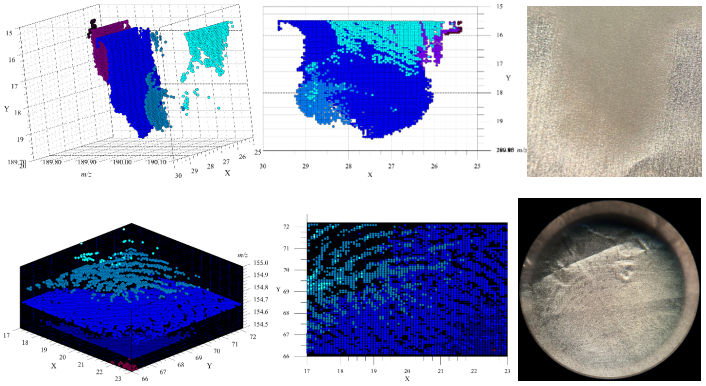

Figure 4. Comparison of MALDI-image (Δ-TOF, threshold 60 %, *m/z* 189.7-190.1, total of 2030 profiles, area: 4.21 x 4.34 mm) to microscopic picture of spot sampled. Top row: The topography of the deposited CHCA matrix on aluminum foil correlated with the observed minute differences in flight time. Thinner matrix layer (lower left and upper right in the microscopic picture) resulted in higher *m/z*-values (cyan). Thicker matrix layer in the center diagonal resulted in lower *m/z*-values (blue). Bottom row: Δ-TOF of a human fingerprint (threshold 80 %, *m/z* 154.5-155.0, total of 5775 profiles, area: 6.03 x 5.98 mm).

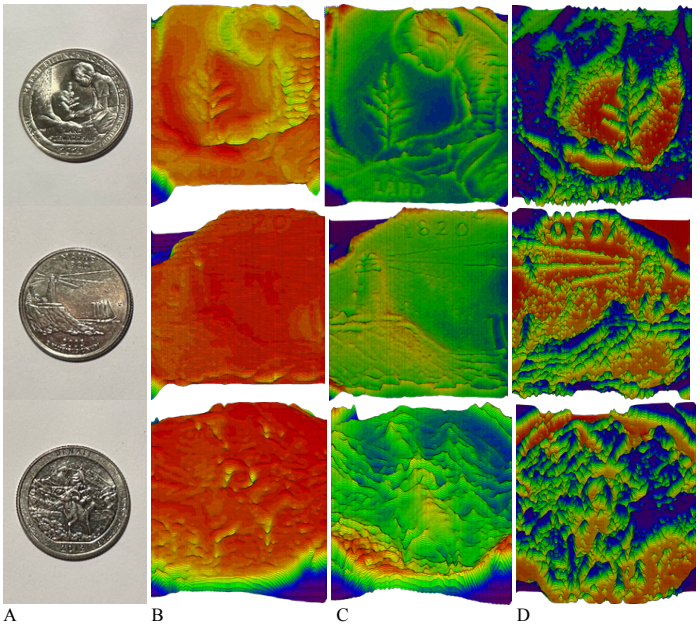

Figure 5. A: Coin used for MALDI-Δ-TOF imaging. B: Total Ion Current (TIC) detected during data acquisition. C: Extracted image at *m/z* 188.8 ± 0.1. D: Image from extracted *m/z* range 188.7-189.6 within 1 *m/z* unit to avoid overlap with ^{13}C-isotope peak.

pulses per spot prevent "hole burning" and variations in the measured flight times that can lead to erroneous "depth" information in the Δ-TOF image. The sublimed matrix gave strong ion response (TIC) across the entire surface (Fig. 5B). When we extracted images for specific *m/z*-values, for example *m/z* 188.8 (Fig. 5C), details of the coin were clearly visible. However, it was only intensity-dependent data that created the image. Conversion of the images to Δ-TOF format revealed the correct surface profile with elevations and depressions clearly visible in the mirror image. We noticed that details were not as well resolved in some areas as in other. For example, the commemorative coin for land stewardship featured a more iconographic picture with larger uniform surface features (Fig. 5, top) as opposed to the coin for Denali National Park and Preserve that included a landscape with closely spaced minute surface differences (Fig. 5, bottom). Such minor differences were easy for the human eye or a light microscope to pick up without ambiguity. However, the current Δ-TOF method seemed to have limitations resolving such minor differences.

Whereas the spatial resolution of the laser beam of ~80 mm (see above) should have been sufficient for acceptable detail, the resolution limit in Δ-TOF was possibly caused by three factors. First, the ratio of elevation/depression of the surface; sharp edges were easily imaged whereas subtle elevation transitions were sometimes missed. More clearly embossed images and image features led to better results. Second, uniform matrix deposition during resublimation; deposition onto the surface is a complex process including heat transfer and crystal formation, which might have caused uneven matrix distribution and blurred the result in Δ-TOF as a consequence. Third, space-charge effects during desorption; the Δ-TOF method described here operated under the oversimplified assumption that all ions are desorbed/ionized off the surface without any effect from adjacent locations on the surface. The absorption of laser light energy is known to involve multiple processes such as multi-photon ionization (MPI),[24] gas-phase cluster ionization leading to "lucky survivors",[25-27] and thermal proton transfer with different ion-to-neutral ratios.[26-27] These processes can be decoupled leading to new MALDI technologies.[30] It has even become apparent recently that thermal processes possibly make the use of laser light unnecessary and Matrix-Assisted Ionization (MAI) is possible.[31-32]

Conclusion

The MALDI-Δ-TOF method for topographic surface characterization requires TOF precision but not *m/z* accuracy. Here we have provided proof of concept with a single "reporter" ion generated from the MALDI matrix. However, in principle, a chosen reporter ion for imaging can have any *m/z*-value and can be picked from the recorded spectrum. This implies that the MALDI-Δ-TOF method has the potential to allow multi-component topographic surface analysis. Current temperature limitations in matrix deposition that deteriorates biological samples need to be addressed in future experiments. If Δ-TOF can be adapted to biological objects, it has the potential to reveal surface topography and spatial distribution of sample/tissue-specific compounds whose identities would require fragmentation techniques because mass accuracy is, by definition, not a feature of Δ-TOF. Together with well-established techniques such as CLSM, Δ-TOF can potentially contribute additional information about specific compounds and could serve as an ancillary analytical technique to microscopy. Validation of differences in thickness measured by Δ-TOF will require surface data from a point micrometer or from CLSM. The measurements can then be compared and quantitatively evaluated. Efforts toward this goal are currently underway in our laboratory.

References

1. Karas, M.; Bachmann, D.; Hillenkamp, F., *Anal. Chem.* **1985**, *57* (14), 2935-2939, https://doi.org/10.1021/ac00291a042.
2. Stevens, W. E., *Phys. Rev.* **1946**, *69* (11-12), 674-674, https://doi.org/10.1103/PhysRev.69.674.
3. Mirsaleh-Kohan, N.; Robertson, W. D.; Compton, R. N., *Mass Spectrom. Rev.* **2008**, *27* (3), 237-285, https://doi.org/https://doi.org/10.1002/mas.20162.
4. Tanaka, K.; Waki, H.; Ido, Y.; Akita, S.; Yoshida, Y.; Yoshida, T.; Matsuo, T., *Rapid Commun. Mass Spectrom.* **1988**, *2* (8), 151-153, https://doi.org/https://doi.org/10.1002/rcm.1290020802.
5. Nobel Prize in Chemistry. https://www.nobelprize.org/prizes/chemistry/2002/summary/ (accessed December 24).
6. Lamy, B.; Sundqvist, M.; Idelevich, E. A., *Clin. Microbiol. Inf.* **2020**, *26* (2), 142-150, https://doi.org/10.1016/j.cmi.2019.11.017.
7. Sauget, M.; Valot, B.; Bertrand, X.; Hocquet, D., *Trends Microbiol.* **2017**, *25* (6), 447-455, https://doi.org/10.1016/j.tim.2016.12.006.
8. Idelevich, E. A.; Becker, K., *Clin. Microbiol. Inf.* **2019**, *25* (11), 1347-1355, https://doi.org/10.1016/j.cmi.2019.04.025.
9. Oviaño, M.; Bou, G., *Clin. microbiol. Rev.* **2019**, *32* (1), https://doi.org/10.1128/cmr.00037-18.
10. Perry, J. D., *Clin. Microbiol. Rev.* **2017**, *30* (2), 449-479, https://doi.org/10.1128/cmr.00097-16.
11. Li, D.; Yi, J.; Han, G.; Qiao, L., *ACS Meas. Sci. Au* **2022**, *2* (5), 385-404, https://doi.org/10.1021/acsmeasuresciau.2c00019.
12. Sharin, M. D.; Floro, G. M.; Clark, K. D., *Int. J. Mass Spectrom.* **2023**, *494*, 117138, https://doi.org/https://doi.org/10.1016/j.ijms.2023.117138.
13. Liu, X.; Niu, H.; Guo, D.; Gao, H.; Wu, L.; Liu, J.; Bai, C.; Li, Y.; Wang, P.; Zhou, Z.; Wang, Y.; Liang, J.; Gong, W., *Microbiol. Spectr.* **2025**, *13* (5), e01545-24, https://doi.org/10.1128/spectrum.01545-24.
14. Zhang, S.; Liu, J. a.; Chen, Y.; Xiong, S.; Wang, G.; Chen, J.; Yang, G., *J. Am. Soc. Mass Spectrom.* **2010**, *21* (1), 154-160, https://doi.org/https://doi.org/10.1016/j.jasms.2009.09.024.
15. Herzog, R. F. K.; Viehböck, F. P., *Phys. Rev.* **1949**, *76* (6), 855-856, https://doi.org/10.1103/PhysRev.76.855.
16. Honig, R. E., *J. Appl. Phys.* **1958**, *29* (3), 549-555, https://doi.org/10.1063/1.1723219.
17. Ievlev, A. V.; Belianinov, A.; Jesse, S.; Allison, D. P.; Doktycz, M. J.; Retterer, S. T.; Kalinin, S. V.; Ovchinnikova, O. S., *Scientific Reports* **2017,** *7* (1), 17099, https://doi.org/10.1038/s41598-017-17049-y.
18. Bejjani, A.; Noun, M.; Della-Negra, S.; Tannous, R.; Chalhoub, G.; Hamdan, M.; Nsouli, B., *Analytical Chemistry* **2019,** *91* (14), 8864-8872, https://doi.org/10.1021/acs.analchem.9b00114.
19. Trim, P. J.; Snel, M. F., *Methods* **2016**, *104*, 127-141, https://doi.org/https://doi.org/10.1016/j.ymeth.2016.01.011.
20. Noun, M.; Akoumeh, R.; Abbas, I., *Microsc. Microanal.* **2022**, *28* (1), 1-26, https://doi.org/10.1017/S1431927621013593.

21. Passarelli, M. K.; Winograd, N., *Surf. Interface Anal. : SIA* **2011**, *43* (1-2), 269-271, https://doi.org/10.1002/sia.3529.
22. Spears, I.; Lagdameo, G.; Black, A.; Brown, D. R.; Johnson, C. C.; Hahm, T.-H.; Wang, W.; Creissen, A.; Glunde, K.; Tressler, C. M., *Anal. Chem.* **2025**, *97* (35), 19001-19008, https://doi.org/10.1021/acs.analchem.5c01767.
23. Stauber, J. M.; Wilson, S. K.; Duffy, B. R.; Sefiane, K., *Langmuir* **2015**, *31* (12), 3653-3660, https://doi.org/10.1021/acs.langmuir.5b00286.
24. Zenobi, R.; Knochenmuss, R., *Mass Spectrom. Rev.* **1998**, *17* (5), 337-366, https://doi.org/https://doi.org/10.1002/(SICI)1098-2787(1998)17:5.
25. Karas, M.; Glückmann, M.; Schäfer, J., *J. Mass Spectrom.* **2000**, *35* (1), 1-12, https://doi.org/https://doi.org/10.1002/(SICI)1096-9888(200001)35:1<1::AID-JMS904>3.0.CO;2-0.
26. Karas, M.; Krüger, R., *Chem. Rev.* **2003**, *103* (2), 427-440, https://doi.org/10.1021/cr010376a.
27. Knochenmuss, R., *Annu. Rev. Anal. Chem.* **2016**, *9* (Volume 9, 2016), 365-385, https://doi.org/https://doi.org/10.1146/annurev-anchem-071015-041750.
28. Tsai, M.-T.; Lee, S.; Lu, I. C.; Chu, K. Y.; Liang, C.-W.; Lee, C. H.; Lee, Y. T.; Ni, C.-K., *Rapid Commun. Mass Spectrom.* **2013**, *27* (9), 955-963, https://doi.org/https://doi.org/10.1002/rcm.6534.
29. Lu, I.-C.; Lee, C.; Lee, Y.-T.; Ni, C.-K., *Annu. Rev. Anal. Chem.* **2015**, *8* (Volume 8, 2015), 21-39, https://doi.org/https://doi.org/10.1146/annurev-anchem-071114-040315.
30. Soltwisch, J.; Kettling, H.; Vens-Cappell, S.; Wiegelmann, M.; Müthing, J.; Dreisewerd, K., *Science* **2015**, *348* (6231), 211-215, https://doi.org/10.1126/science.aaa1051.
31. Trimpin, S., *J. Am. Soc. Mass Spectrom.* **2016**, *27* (1), 4-21, https://doi.org/10.1007/s13361-015-1253-4.
32. Peacock, P. M.; Zhang, W.-J.; Trimpin, S., *Anal. Chem.* **2017**, *89* (1), 372-388, https://doi.org/10.1021/acs.analchem.6b04348.

Supplemental Material

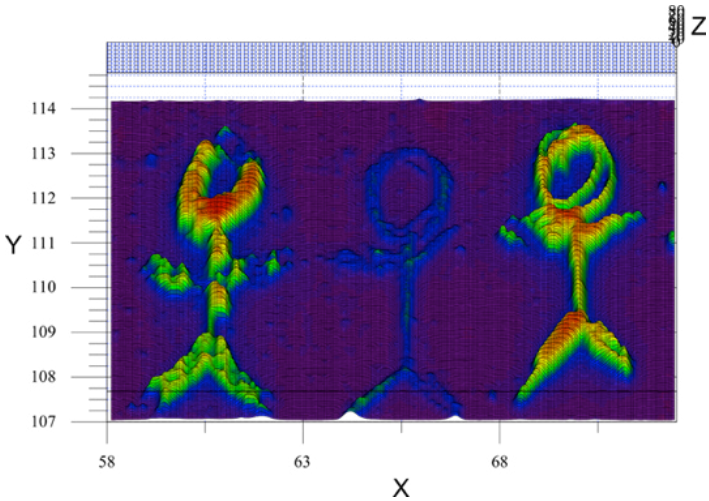

Figure S1. Left: MALDI-images of three stick figure drawings with BIC ballpoint pen (left to right: black, red, and blue; Z-axis: TIC ion count) on the MALDI target plate. Resolution ~80 mm (see Fig. S2).

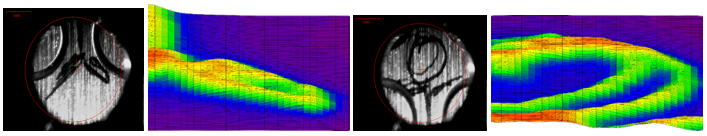

Figure S2. Detail of blue stick figure from camera picture and MALDI-image (left: leg; right: head) demonstrating the ability to resolve line spacing of ~80 mm

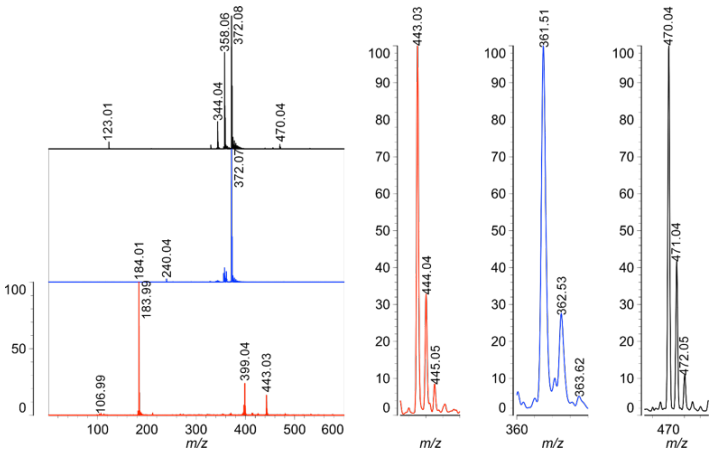

Figure S3. MALDI-TOF mass spectra of red ink, blue ink, and black ink. The unique ions to each ink are shown to the right.

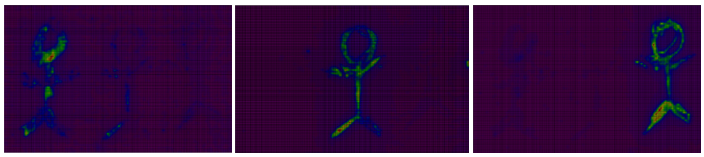

Figure S4. Extracted ion images for *m/z* 361 (unique for black), *m/z* 443 (unique for red), and *m/z* 470 (unique for blue).

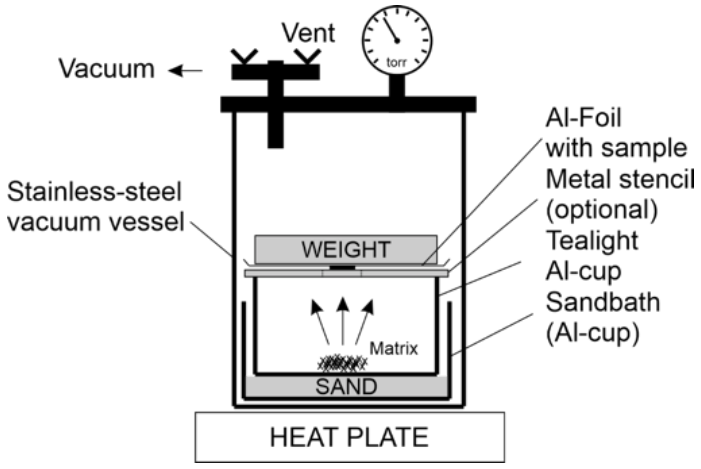

Figure S5. Schematic view of sublimation apparatus. The temperature of the external heat plate under the stainless-steel vacuum vessel was ~180-200 °C. The layer of sand was only ~5 mm thick; enough to allow more uniform heat transfer from the bottom of the vessel to the tea light Al-cup whose floor was not entirely planar.

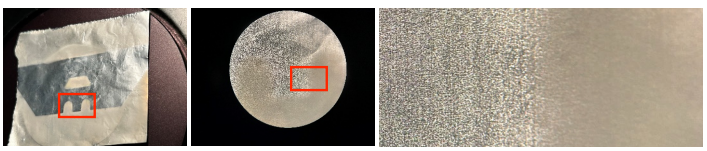

Figure S6. Sublimation of CHCA onto aluminum foil with box cutter blade stencil. Oil pump vacuum, 200 °C, 5 minutes. Note the excellent microscopic size of matrix crystals that are smaller than the surface texture of the aluminum foil (right).

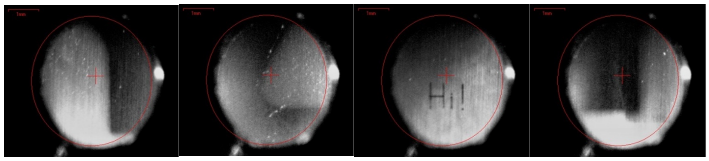

Figure S7. Instrument camera pictures. From left to right: matrix deposit outlining the capsule shape of the box cutter blade, matrix deposit outlining the trapezoid shape of the box cutter blade, pattern burned into the thin matrix layer by the laser, and visual matrix depletion during imaging of the capsule shape. The matrix layer was thick enough to withstand ~10 laser pulses before depletion of material.

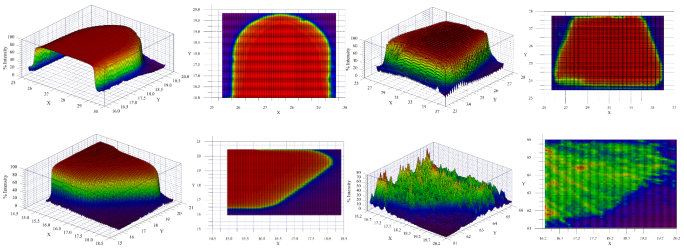

Figure S8. MALDI-images of matrix deposits created by the box cutter blade stencil. Top row: TIC, CHCA matrix, laser power 70; bottom row left: TIC, DHB matrix, laser power 80. Ionization was near uniform across both surfaces and was reproducible. Bottom row right: TIC, 3-HPA matrix, only 2 minutes of sublimation, laser power 80.

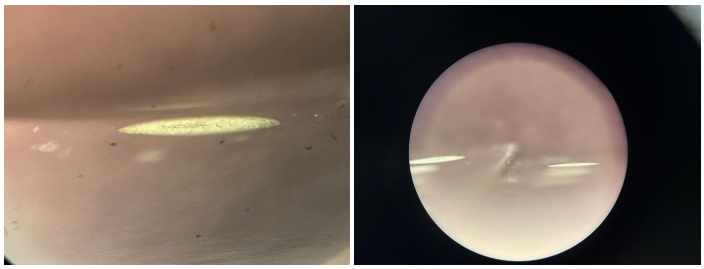

Figure S9. Microscopic picture of two dried droplets (CHCA matrix) on a stair step.

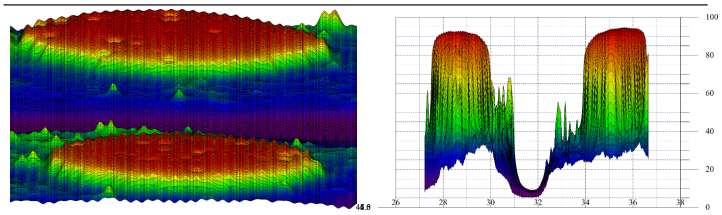

Figure S10. Left: Total ion image of two CHCA dried droplets, each on a different step of the staircase. The spot towards the back was on a higher step of the staircase. Signal intensity was excellent across each crystal surface. Right: Profile view of the same two spots along the x-axis. Without prior knowledge, it would not be possible to discern which profile resulted from the spot lower or higher on the staircase.

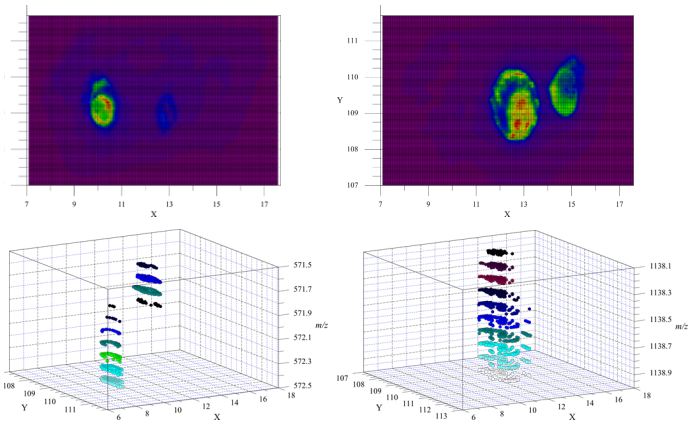

Figure S11. MALDI-TOF analysis (CHCA matrix, threshold 50 %) of three evaporated droplets containing bradykinin ([M+H]$^+$ *m/z* 573) and gramicidin S ([M+H]$^+$ *m/z* 1041). Left droplet: bradykinin only, center droplet: bradykinin and gramicidin S (equimolar), right droplet: gramicidin S only. Top: MALDI-TOF image by TIC. Bottom: MALDI-Δ-TOF image. The effect of "hole burning" (progressively longer flight times with increasing number of laser pulses) and suppression of bradykinin by gramicidin S in the mixture was obvious.